Journal of Non-Crystalline Solids 454 (2016) 39–45

Contents lists available at ScienceDirect

Journal of Non-Crystalline Solids

journal homepage: www.elsevier.com/locate/jnoncrysol

Thermal stability, crystallization and soft magnetic properties of Fe-P-C-based glassy alloys

Jianfeng Wang [a,*], Yaxin Di [a], Zhe Fang [a], Shaokang Guan [a], Tao Zhang [b]

[a] School of Materials Science and Engineering, Zhengzhou University, Zhengzhou 450001, PR China
[b] School of Materials Science and Engineering, Beihang University, Beijing 100191, PR China

ARTICLE INFO

Article history:
Received 24 July 2016
Received in revised form 11 September 2016
Accepted 16 October 2016
Available online xxxx

Keywords:
Iron alloys
Metallic glasses
Crystallization
Magnetic properties

ABSTRACT

Thermal stability, crystallization and magnetic properties of $Fe_{80}P_{11}C_9$, $Fe_{80}P_9B_2C_9$, and $Fe_{77}Al_3P_9B_2C_9$ glassy alloys were investigated. The relationships of glass-forming ability (GFA) with thermal properties and crystallization, magnetic properties with crystallization were also discussed. The variation trend of GFA for these glassy alloys is in agreement with the reduced glass transition temperature. The annealing experiment shows that the primary precipitation phase both for the $Fe_{80}P_{11}C_9$ and $Fe_{80}P_9B_2C_9$ glassy alloys is α-Fe, and the addition of small amounts of Al is effective for suppression of the formation of α-Fe phase, resulting in the extension of supercooled liquid region and significant enhancement of GFA. The activation energy for primary crystallization calculated by Kissinger's equation indicates the addition of B in Fe–P–C alloy or Al in Fe–P–B–C alloy makes nucleation more difficult, which is responsible for the enhancement of GFA. In addition, it was found that the crystallized $Fe_{80}P_9B_2C_9$ specimen with ultrafine α-Fe grains exhibits high saturation magnetic polarization of up to 1.60 T and low coercive force of about 3.0 A/m.

1. Introduction

Fe-based amorphous alloys and the corresponding nanocrystalline alloys are of great value for commercial applications due to their excellent soft magnetic properties including high saturation magnetic polarization (J_s), low coercive force (H_c), and high permeability (μ) [1,2]. In recent decades, Fe-based ferromagnetic amorphous foils have been widely used as key parts in magnetic devices, such as high-efficiency transformers and sensors. In order to further extend their application fields as magnetic materials, many efforts have been devoted to developing new Fe-based ferromagnetic glassy alloys with better glass-forming ability (GFA). For the last decades, a number of Fe-based ferromagnetic bulk metallic glasses (BMGs) have been synthesized, which can be broadly categorized into three groups. One is Fe–P–C-based BMG group [3–14], another is Fe–B–Si-based BMG group [15–20], and the other is Fe–B-based BMG group [21–26]. Among these types, Fe–P–C-based BMGs have attracted increasing interests for their promising mechanical and magnetic properties, such as $(Fe,Mo,Ni,Cr)_{80}P_{12.5}C_5B_{2.5}$ BMGs with notch toughness values of 44.2–53.1 MPa·$m^{1/2}$ [12], $Fe_{74-x}Mo_xP_{13}C_7$ ($x = 3$ and 6) BMGs with plastic strain (ε_p) of above 5.0% [14], and $Fe_{81}Mo_1P_{7.5}C_{5.5}B_2Si_3$ and $Fe_{82}Mo_1P_{6.5}C_{5.5}B_2Si_3$ BMGs with saturation magnetization of about 1.6 T [13,14]. It is especially noted that some of these BMGs, such as $Fe_{76}Mo_2P_{10}C_{7.5}B_{2.5}Si_2$ [10], $Fe_{78}Mo_1P_9C_{6.5}B_{3.5}Si_2$ [13], and $Fe_{77}Mo_3P_{13}C_7$ [14] were reported to exhibit a unique combination of high J_s and appreciable ε_p. Such alloys could be more viable for use directly in bulk form as magnetic sensors, valves, and clutches. However, these alloys contain relatively expensive metallic element Mo, which leads to a significant increase in materials cost.

Recently, considering that the raw material cost of Fe-based glassy alloys is very important for their practical applications, we have developed a Mo-free $Fe_{80}P_{11}C_9$ BMG with a critical diameter of 1.5 mm by copper mold casting in ternary Fe–P–C alloy system [27]. The alloy with a lower materials cost (compared with Mo-bearing Fe–P–C-based BMGs) exhibits good overall properties, such as high J_s of up to 1.37 T and significant ε_p of about 1.4%. Although Li et al. [28] also reported that a ternary $Fe_{80}P_{13}C_7$ BMG with J_s of 1.53 T and ε_p of about 1.1% can be synthesized by the combination of fluxing treatment and J-quenching technique at the same time, the preparation process of BMGs is more complicated. Subsequently, we designed new $Fe_{80}P_9B_2C_9$ [29] and $Fe_{77}Al_3P_9B_2C_9$ [30] BMGs with a better combination of GFA and properties by adding B and Al into Fe–P–C and Fe–(P,B)–C alloys, respectively. In this paper, we intend to further investigate the substitution effects of B and Al elements on the thermal properties, crystallization and soft magnetic properties of Fe–P–C-based glassy alloys. In addition, the relationships of GFA with thermal properties and crystallization, soft magnetic properties with crystallization were also discussed.

2. Experimental

Mother alloy ingots with nominal compositions of $Fe_{80}P_{11}C_9$, $Fe_{80}P_9B_2C_9$, and $Fe_{77}Al_3P_9B_2C_9$ were prepared by induction melting the mixture of pure Fe (99.9 mass%), Al (99.9 mass%), C (99.99 mass%),

* Corresponding author.
E-mail address: jfwang316@zzu.edu.cn (J. Wang).

http://dx.doi.org/10.1016/j.jnoncrysol.2016.10.014
0022-3093/

and pre-alloyed Fe–P (22.41 mass% P) and Fe–B (17.24 mass% B) in a purified argon atmosphere. The weight loss due to melting was found to be less than 0.15% of the starting materials. Alloy ribbons with a dimension of about 20 μm in thickness and about 1.0 mm in width were prepared by single-roller melt spinning. Alloy rods with different diameters of 1.0–3.0 mm and a length of a couple of centimeters were prepared by copper mold casting.

The glassy and crystallized structures were identified by X-ray diffraction (XRD) with Cu Kα radiation. Glass transition, crystallization, and melting behaviors were evaluated using differential scanning calorimetry (DSC) at a heating rate of 20 K/min. To reduce the influence of undercooling, the solidification behavior was investigated using DSC at a very low cooling rate of 5 K/min. The crystallization kinetics of each as-spun specimen was evaluated using DSC at different heating rates of 10, 20, 30, and 40 K/min. The annealing experiment was carried out by keeping the as-spun amorphous specimens in the tubular furnace preheated to annealing temperatures for 600 s under vacuum atmosphere followed by water quenching. The density was measured by Archimedes' method. The saturation magnetic polarization (J_s) and coercive force (H_c) were measured at room temperature with a vibrating sample magnetometer (VSM) under an applied field of 150 kA/m. For alloys with a smaller H_c than 100 A/m, H_c was measured by a DC B-H loop tracer under a field of 400 A/m.

3. Results

3.1. Thermal stability

Fig. 1(a)–(c) display DSC curves of the melt-spun $Fe_{80}P_{11}C_9$, $Fe_{80}P_9B_2C_9$, and $Fe_{77}Al_3P_9B_2C_9$ glassy alloys at different heating rates from 10 to 40 K/min showing the glass transition and crystallization behaviors. Upon heating, each of the curves exhibits an obvious endothermic event characteristic of the glass transition and a supercooled liquid region, followed by exothermic reactions corresponding to the crystallization of the undercooled liquid. From Fig. 1(a) and (b), the $Fe_{80}P_{11}C_9$ and $Fe_{80}P_9B_2C_9$ glassy alloys exhibit a weak exothermic shoulder peak before the main exothermic peak which is caused due to the overlapping of two crystallization peaks. The substitution of 3 at.% Fe by Al in $Fe_{80}P_9B_2C_9$ alloy leads to disappearing of the shoulder peak as shown in Fig. 1(c). The values of the glass transition temperature (T_g) and onset crystallization temperature (T_x) determined from the DSC traces of 20 K/min heating rate are summarized in Table 1. Both T_g and T_x increase with substitution of 2 at.% P by B element in $Fe_{80}P_{11}C_9$ alloy as well as with further substitution of 3 at.% Fe by Al in $Fe_{80}P_9B_2C_9$ alloy. The melting and solidification behaviors of these alloys are shown in Fig. 2. The near invariance of T_m for these compositions indicates that they may have the same eutectic reaction. Upon cooling, the $Fe_{80}P_{11}C_9$ alloy shows two exothermic peaks. The first peak at the high temperature corresponds to the solidification of the primary phases, while the second one at the relatively low temperature is ascribed to that of the eutectic phase. When compared with $Fe_{80}P_{11}C_9$ alloy, the first peak for $Fe_{80}P_9B_2C_9$ alloy is shifted to a lower temperature, which leads to the overlapping of two peaks in the DSC curve. Consequently, T_l is also lowered from 1262 to 1240 K as shown in Table 1. The further decrease of T_l is caused by the addition of Al element. Therefore, it is suggested that $Fe_{77}Al_3P_9B_2C_9$ alloy with the lowest T_l is the closest to the eutectic point among these three alloys.

3.2. Crystallization behavior

Fig. 3(a)–(c) shows XRD patterns of $Fe_{80}P_{11}C_9$, $Fe_{80}P_9B_2C_9$, and $Fe_{77}Al_3P_9B_2C_9$ glassy alloys subjected to annealing for 600 s at different temperatures. The XRD patterns of as-spun specimens are also shown for comparison. Obviously, after annealing at (T_g − 20) K, these alloys maintain glassy structure. As we have known, the isothermal heat treatment in the supercooled liquid region can induce phase separation,

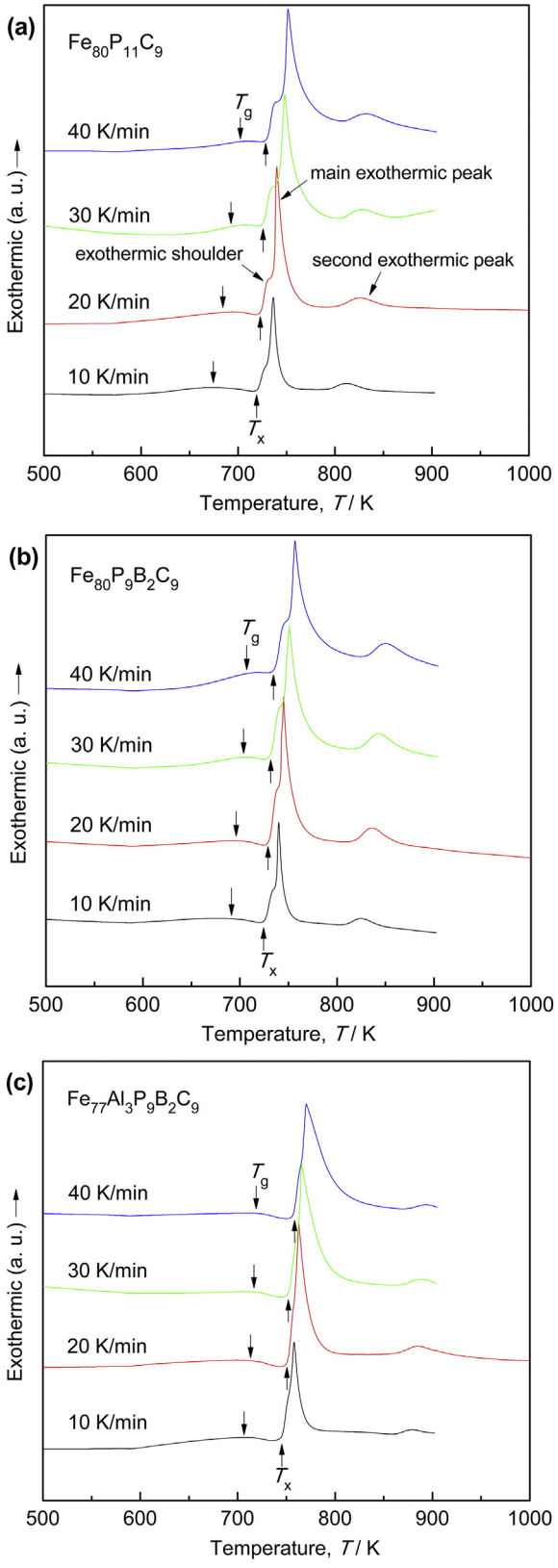

Fig. 1. DSC curves of (a) $Fe_{80}P_{11}C_9$, (b) $Fe_{80}P_9B_2C_9$, and (c) $Fe_{77}Al_3P_9B_2C_9$ glassy alloys at different heating rates from 10 to 40 K/min, showing glass transition and crystallization behaviors. Arrows indicate the glass transition temperature (T_g) and onset crystallization temperature (T_x), respectively.

nucleation, and growth of nuclei. For $Fe_{80}P_{11}C_9$ alloy, as shown in Fig. 3(a), α-Fe phase primary precipitates from the glassy matrix after annealed at 695 K and 700 K in the supercooled liquid region. The result